Environmental Science & Technology

pubs.acs.org/est

Article

Efficient Atmospheric Transport of Microplastics over Asia and Adjacent Oceans

Xin Long, Tzung-May Fu,* Xin Yang, Yuanyuan Tang, Yan Zheng, Lei Zhu, Huizhong Shen, Jianhuai Ye, Chen Wang, Teng Wang, and Baojie Li

Cite This: *Environ. Sci. Technol.* 2022, 56, 6243−6252

Read Online

ACCESS | Metrics & More | Article Recommendations | Supporting Information

ABSTRACT: We developed a regional atmospheric transport model for microplastics (MPs, 10 μm to 5 mm in size) over Asia and the adjacent Pacific and Indian oceans, accounting for MPs' size- and shape-dependent aerodynamics. The model was driven by tuned atmospheric emissions of MPs from the land and the ocean, and the simulations were evaluated against coastal (n = 19) and marine (n = 56) observations. Our tuned atmospheric emissions of MPs from Asia and the adjacent oceans were 310 Gg y^{-1} (1 Gg = 1 kton) and 60 Gg y^{-1}, respectively. MP lines and fragments may be transported in the atmosphere >1000 km; MP pellets in our model mostly deposited near-source. We estimated that 1.4% of the MP mass emitted into the Asian atmosphere deposited into the oceans via atmospheric transport; the rest deposited over land. The resulting net atmospheric transported MP flux from Asia into the oceans was 3.9 Gg y^{-1}, twice as large as a previous estimate for the riverine-transported MP flux from Asia into the oceans. The uncertainty of our simulated atmospheric MP budget was between factors of 3 and 7. Our work highlighted the impacts of the size and morphology on the aerodynamics of MPs and the importance of atmospheric transport in the source-to-sink relationship of global MP pollution.

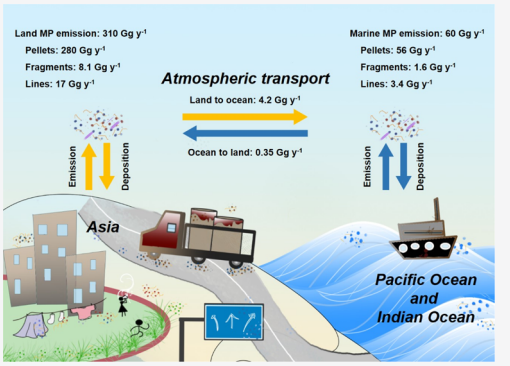

KEYWORDS: *microplastic pollution, atmospheric transport, WRF-MP, microplastic emission, microplastic deposition*

INTRODUCTION

Microplastics (MPs) are small plastic particles <5 mm in size.[1] MPs may be released to the environment from primary or secondary sources.[1] Primary MPs are purposely manufactured for specific uses (e.g., abrasive agents).[1] Secondary MPs are formed by the wear and tear or fragmentation of larger plastic objects, both during their use and following their loss to the environment.[1] MPs have been detected in a variety of natural environments, including the air, soil, fresh waters, surface oceans, sediments, biota, and human tissues.[2−5] The environmental and health risks associated with these MP exposures are still uncertain,[6] with research findings ranging from no effects to mortality of biota.[7−11] Nevertheless, the global sources and the potential adverse impacts of MPs are expected to grow with the increasing use of plastic materials unless effective mitigation measures are implemented.[12]

The transport pathways of MPs from their anthropogenic sources to remote environments are not well understood.[13−16] Previous studies mostly attributed MPs in the surface ocean to the riverine outflow of larger plastic debris, which then breaks down in the surface ocean.[15−20] However, recent studies have observed MPs over remote lands or water bodies lacking local discharge sources or riverine inputs,[21] including remote mountain catchments,[15,22,23] Arctic and Antarctic snow,[24,25] deep-sea polar ecosystems,[26,27] and in the surface air over the remote Pacific and Indian oceans.[28,29] These observations indicate that MPs may be transported by the atmosphere over long distances.

To date, only a few model studies have investigated the characteristics of the atmospheric transport of MPs and the extents to which atmospheric depositions contribute to MPs' presence in ecosystems.[30,31] A critical aspect of complexity is that MPs are present in the environment in a wide range of sizes, shapes, and densities.[1,32] These physical properties can affect MPs' aerodynamics and deposition from the atmosphere. For example, heavy MPs quickly settle from the air and may not be transported far from their sources.[30] In comparison, MPs that are lighter or with larger surface-to-volume ratios (e.g., lines, films, and fragments) may settle more slowly, allowing them to be transported in the atmosphere over longer distances. A Lagrangian model study estimated that 30% of the global MPs produced by road traffic were transported by the atmosphere to deposit into the oceans.[31] However, that study

Received: November 17, 2021
Revised: April 15, 2022
Accepted: April 18, 2022
Published: April 28, 2022

focused on spherical MPs in a limited size range of 0.5−9.5 μm, and the simulated results were not evaluated due to a lack of relevant observations. Brahney et al.[30] simulated the atmospheric transport of MP spheres and fibers (0.3−70 μm in effective diameter) in a general circulation model, constrained by the observed deposited atmospheric MP fluxes at 11 sites in the Western U.S. That study estimated the atmospheric residence times of MPs to be between 0.04 and 6.5 days. Brahney et al.[30] suggested that marine MP sources may dominate the global atmospheric deposition of MPs and that most continents were net importers of atmospheric MPs from the global oceans. However, their model did not explicitly simulate the aerodynamics of MPs of different shapes. Also, the regional measurements used to constrain their model mainly represented atmospheric MPs in the Western U.S., such that extrapolations to world regions were uncertain.

We present here a regional atmospheric transport model of MPs (~10 μm to 5 mm) over Asia and the adjacent areas of the Pacific and Indian Oceans (40°E to 170°E, 12°S to 55°N; domain shown in Figure 1). We simulated the size- and shape-dependent aerodynamics of MPs, which affected their emissions into the atmosphere and subsequent transport and deposition efficiencies. We tuned and evaluated our model using regional measurements of atmospheric MPs over Asia and the adjacent oceans, with the goal of quantifying the source-to-sink relationships of MPs between land and oceans in this region.

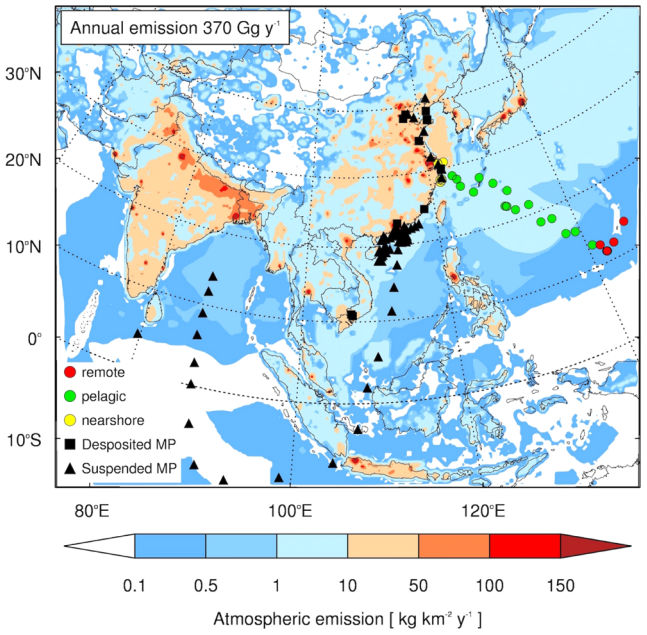

Figure 1. Tuned atmospheric emissions of MPs over Asia and its adjacent areas of the Pacific and Indian oceans for the year 2018. The annual total atmospheric MP emission over the domain was 370 Gg y^{-1}. Colored dots indicate the locations of the suspended atmospheric MP measurements from Liu et al.:[28] near-shore (yellow), pelagic (green), and remote (red). Also shown are the locations of the other suspended atmospheric MP[29,34,37,38] (triangles) and deposited atmospheric MP measurements[33−36] (squares) used for model evaluation.

DATA AND METHOD

Measurements of Atmospheric MPs over Asia and the Pacific and Indian Oceans. As a guide to our model construction and for tuning the atmospheric emissions of MPs in our model, we used the measurements of suspended atmospheric MPs (MPs suspended in the air at the time of sampling) over the Northwestern Pacific Ocean during November 24, 2018 to January 2, 2019 by Liu et al.[28] The measurements were taken on board a ship cruising from Shanghai to the Mariana Islands. A total of 89 air samples were collected at 42 locations; each location was categorized as near-shore, pelagic, or remote, based on its distance from the Asian coast (Figure 1). From these samples, 206 MPs (16−2086 μm in length) were identified. The observed MPs showed four distinct shapes, which the researchers described as microbeads (i.e., spherical MPs), granules (slightly irregular spherical MPs), fragments, and fibers.[28] To reduce confusion arousing from inconsistent terminology, we referred to these shapes as pellets (combining microbeads and granules), fragments, and lines, following the recommendations from the Joint Group of Experts on the Scientific Aspects of Marine Environmental Protection.[1] MP lines were the most abundant, followed by fragments and pellets.[28] To the best of our knowledge, Liu et al.[28] was one of only two published measurements that reported the abundances of suspended atmospheric MPs at near-source and remote locations while also providing size/morphology information. This information should help manifest the impacts of size/morphology on the atmospheric transport of MPs.

We evaluated our simulations against additional measurements of suspended atmospheric MP concentrations[33−36] and deposited atmospheric MP fluxes (fluxes of MPs deposited from the atmospheres)[29,34,37,38] at 19 East Asian coastal sites and 56 locations in the Indian Ocean and the South China Sea (Figure S1 and Table S1). The deposited MP fluxes were measured between October 2016 and June 2019 by four different research groups using generally consistent sampling and analytical methods.[33−36] The suspended MP concentrations were measured between October 2018 and July 2020 by two research groups using consistent analytical methods but with different sampling instruments and sampling durations.[33−36] At Lianyungang and Tianjin, measurements of suspended atmospheric MPs and deposited atmospheric MP fluxes were both available. However, the measurements were not sampled concurrently and analyzed with different methods[28,34] (Figure S1 and Table S1). All measurements of suspended and deposited atmospheric MPs used in this study found MP lines to be the dominant shape by both number and mass (Table S1). Polyethylene terephthalate[28,29,34,35,37,38] and cellophane[35] were the main polymer types in the observed MPs.

Development of the WRF-MP Model and Simulation of MPs' Atmospheric Transport. We constructed an aerodynamics module for MPs and coupled it online to the Weather Research and Forecasting (WRF) model. This new model, hereafter referred to as WRF-MP, simulated the atmospheric processes of MPs, including their emissions, transport (advection, convective, and turbulent mixing) (Text S1), and removal (dry deposition and wet scavenging). WRF-MP was developed based on the framework of the WRF-Dust model,[39,40] which has been used extensively to simulate the atmospheric transport of dust.[41−43] MPs were represented in

https://doi.org/10.1021/acs.est.1c07825
Environ. Sci. Technol. 2022, 56, 6243−6252

WRF-MP as size-segregated, insoluble aerosols, similar to the treatment of dust in WRF-Dust.[43]

The aerodynamics of an MP particle depends on its size, shape, and density. Guided by the observations of Liu et al.,[28] we represented MPs in WRF-MP with 8 particle bins of different shapes and sizes (Table S2): P_{40} and P_{70} (pellets with diameters <50 and >50 μm, respectively); F_{60}, F_{150}, and F_{260} (fragments with lengths along the longest dimension <100, 100−200, and >200 μm, respectively); and L_{130}, L_{320}, and L_{900} (lines with lengths <200, 200−500, and >500 μm, respectively). The subscript denoting each particle bin indicated its characteristic dimension (diameter or length in micrometers), taken from the mean observed values from Liu et al.[28] (Table S2). Pellets were treated as spherical particles. Fragments and lines were treated as cuboids and cylinders, respectively.

Similar to dust,[39] MPs in the atmosphere are efficiently removed by gravitational settling due to their large sizes. The gravitational settling velocity of MPs (V_g) was calculated as

$$V_g^2 = \frac{4\cdot(\rho' - 1)\cdot g\cdot d_e}{3\cdot C_d} \quad (1)$$

where ρ' was the particle-to-air density ratio; g was the acceleration of gravity. ($d_e = \sqrt[3]{6\cdot V/\pi}$) was the equivalent spherical diameter with the same volume V as the particle, and C_d was the drag coefficient. We iteratively determined C_d and V_g using a parameterization dependent on the Reynolds number (R_e)[44,45]

$$C_d = \frac{24\cdot K_s}{R_e}\left[1 + 0.125\cdot\left(\frac{R_e\cdot K_N}{K_S}\right)^{2/3}\right] + \frac{0.46\cdot K_N}{1 + 5330/(R_e\cdot K_N/K_S)} \quad (2)$$

$$K_S = [(f\cdot e^{1.3})^{1/3} + (f\cdot e^{1.3})^{-1/3}]/2 \quad (3)$$

$$K_N = 10^{\alpha\cdot[-\log(f^2\cdot e)]^{\beta}} \quad (4)$$

$$Re = \frac{\rho_{air}\cdot V_g\cdot d_e}{\mu} \quad (5)$$

$$\alpha = 0.45 + 10/[\exp(2.5\cdot\log\rho') + 30] \quad (6)$$

$$\beta = 1 - 37/[\exp(3\cdot\log\rho') + 100] \quad (7)$$

where K_S and K_N were the shape-dependent parameters of Stokes' and Newton's drag corrections, respectively, calculated from the flatness ($f = S/I$) and elongation ($e = I/L$) of the particle. L, I, and S were defined as the longest, intermediate, and shortest lengths of the particle, receptively, taken from the measurements of Liu et al.[28,46] (Table S2). The thickness of MP fragments was set to 3 μm (S for F_{60}, F_{150}, and F_{260}),[46] and the average transect diameter of MP lines was set to 10 μm (I and S for L_{130}, L_{320}, and L_{900}). ρ_{air} and μ were the density and dynamics viscosity of air, respectively.[47] We assumed that all MPs in a particle bin were of the same effective size and mean density (Table S2).[46] For the atmospheric MPs considered here, Re ranged from 0.021 to 0.15. The drag coefficient (C_d) calculated from eqs 2−7 has an average error of approximately 10%.[44,45]

We assumed MPs to be hydrophobic and that wet scavenging of MPs involved only the washout by precipitation (Text S1). MPs may become slightly hydrophilic after prolonged UV-aging.[48] However, our simulations showed that wet scavenging contributed <2% of the total atmospheric removal of MPs and thus had only minor effects on the atmospheric transportability of MPs. The spatial pattern of MPs' wet deposition was similar to that of precipitation, with strong monsoonal variations (Figure S2).

We used the WRF-MP model to simulate atmospheric MPs over Asia and the adjacent areas of the Pacific and Indian oceans (40°E to 170°E, 12°S to 55°N; domain in Figure 1). The model horizontal resolution was 36 km. Meteorological initial and boundary conditions are from the National Centers for Environmental Prediction 1° reanalysis data set[49] and updated at the model boundary every 6 h. We assumed that the concentrations of suspended atmospheric MPs at the model boundaries were zero because of the low suspended atmospheric MP concentrations (<0.001 MPs m^{-3}) observed over the remote Pacific and Indian oceans.[29] We first conducted a trial simulation during November 17, 2018 to January 2, 2019 for emission-tuning using the observations by Liu et al.;[28] the model results were sampled at the times and locations of the observations. We then conducted monthly simulations for January, April, July, and October of the year 2018 (each with 7-day spin-up) for evaluation against other atmospheric MP measurements; the model results were sampled at the location of the measurements during the month closest to the measurement time.

The effective size range of MPs represented in our model was determined by the size range of MPs detectable in the measurements used to tune/evaluate the model. Most measurement studies identified MPs as plastic particles <5 mm (Tables S1 and S3). However, the lowest detectable MP sizes varied by experimental protocol, ranging from ∼10 to 300 μm (Tables S1 and S3). As such, the size range of MPs effectively represented in our model was between 10 μm and 5 mm. Most measurements (1) found MP lines to be the dominant MP shape,[28,29,33−38] (2) MP lines were generally >100 μm in length and thus detectable,[28,29,37,38] and (3) the numbers of detected MPs tapered off at large sizes.[28,29,37,38] Our model should therefore represent the bulk of the atmospheric MPs' mass. However, the number of small MPs (<10 μm) might be underestimated in the measurements and in our simulations.

Environmental Emission of MPs from Asia. As a starting point to estimate the Asian atmospheric emissions of MPs, we scaled a Chinese environmental MP emission inventory.[50] This inventory (0.25° resolution, Text S2) estimated the annual total environmental release of MPs from nine primary and secondary sources in Mainland China in 2015 to be 737 Gg (estimated range between 486 and 1160 Gg due to uncertainties associated with emission factors and activity levels).[50]

We estimated the environmental MP emissions from all of Asia for the year 2018 as follows: for each country/region other than Mainland China, we multiplied its population density (0.5° resolution)[51] in 2015 with the regional annual environmental MP emission per capita estimated by Boucher and Friot[13] (Figure S3). We then apportioned the resulting environmental MP emissions to the nine sources using the average source profiles from China.[50] Finally, we scaled the annual total environmental MP emissions for Asia from the

https://doi.org/10.1021/acs.est.1c07825
Environ. Sci. Technol. 2022, 56, 6243−6252

year 2015 to the year 2018, using the global total plastic production for the years 2015 (322 Tg) and 2018 (359 Tg).[52] Our estimate for the total environmental MP emission over land within the simulation domain (Figure 1) was 2400 Gg yr^{-1} in 2018 (uncertainty range 1600−3800 Gg yr^{-1} scaled from the uncertainty of Chinese environmental MP emissions[50]).

We allocated the environmental MP emissions from each of the nine land sources to the eight particle bins in the WRF-MP model (Table S4). There were no quantitative constraints for this allocation; we relied on anecdotal characteristics of the MPs associated with each source activity (Text S3). For example, we assumed that the MPs associated with personal care and cosmetic products were 100% small pellets (P_{40})[53] and that the MPs associated with tire dust were 10% small pellets (P_{40}) and 90% large pellets (P_{70}) by mass. Table S4 summarizes the MP mass allocated to each of the eight particle bins from the anthropogenic land sources (f_i, i = 1 to 8). By mass, 53% of the emitted MPs were allocated to large pellets (P_{70}), mostly as tire dust; 26% of the emitted MP mass was allocated to MP lines (L_{900}), associated with synthetic fibers from clothing and artificial turf.[50] Only 5.9 and 4.1% of the emitted MP mass were allocated to small MP pellets and MP fragments, respectively.

Marine MP Emission Potential. MPs in the surface ocean may be aerosolized into the air through wind or wave actions, similar to the emission process of sea salt aerosols.[54] We defined a marine MP emission potential (P_{sea}, unit: kg m^{-2} s^{-1}) as

$$P_{sea} = C_0 \cdot K_0 \cdot E_0 \tag{8}$$

where E_0 was the wind-dependent flux of sea salt aerosols[55] (unit: kg m^{-2} s^{-1}). K_0 was a global distribution of MP mass concentrations in the surface ocean,[56] normalized to range between 0 and 1 (Figure S4a). C_0 (0.25%) represented the ratio of the global marine MP emission estimated from Brahney et al.[30] (8.6 Tg yr^{-1}, uncertainty range between 0 and 22 Tg yr^{-1} based on limited observational constraints) to the estimated global sea salt (in size range of 0.02−10 μm) emission (3500 Tg yr^{-1}).[57] The morphologies of MPs emitted from the surface ocean into the atmosphere are not well known. We assumed that the f_i of MPs emitted from land also applied to the MPs emitted from the surface ocean, that is, the MP emission potential for the ith particle bin was $P_{i,sea} = f_i \cdot P_{sea}$.

Tuning the Effective Atmospheric Emissions of MPs with Observations. The fraction of MPs entering the atmosphere relative to their total release into the environment is yet unknown and likely varies by the sources, sizes, and shapes of MPs. We defined α_i, the domain-averaged effective fraction of MPs in the ith bin released into the atmosphere relative to their total environmental release

$$\alpha_i \equiv \frac{E_{i,land,atm} + E_{i,sea,atm}}{E_{i,land} + P_{i,sea}} = \frac{N_{i,obs}}{\left(\frac{N_{i,5\%}}{5\%}\right)} \tag{9}$$

where $E_{i,land}$ was the total environmental emission of MPs in the ith bin over land, and $P_{i,sea}$ was the marine emission potential of MPs in the ith bin. $E_{i,land,atm}$ and $E_{i,sea,atm}$, the effective atmospheric emissions of MPs in the ith bin from land and marine sources, respectively, could be estimated with the values of α_i. To tune the values of α_i (eq 9, Text S4), we conducted a trial simulation, arbitrarily assuming that 5% of the total environmental emissions entered the atmosphere. $N_{i,5\%}$ was the trial-simulated number of suspended atmospheric MPs in the ith bin at the times and locations of Liu et al.'s measurements over the Northwestern Pacific.[28] $N_{i,obs}$ was the total number of suspended atmospheric MPs in the ith bin observed by Liu et al.[28] We pooled all samples from Liu et al.[28] without distinguishing the distances of the sampling locations to the Asian coast. We did so because the ratios of suspended atmospheric MPs between coastal, pelagic, and remote sites should be dependent only on the aerodynamics of MPs, which was represented in our model (Text S4 and Figure S5).

Table S5 shows the tuned values of α_i and the resulting estimated atmospheric MP emission for our research domain. The values of α_i were effective and compensated for potential uncertainties associated with many factors, including the environmental MP emission estimates, the shape/size allocation of MPs from different sources, the deposition of MPs from the atmosphere within the model grid of emission, and the atmospheric transport of MPs in our model. In particular, α_i implicitly accounted for some additional secondary emissions of MPs and the re-suspension of MPs previously deposited to the surface by assuming their spatial distributions to be identical to those of the primary sources.

RESULTS

Atmospheric Transportability of MPs of Different Morphologies. MPs in the atmosphere were removed almost entirely by gravitational settling due to their large sizes, such that the gravitational deposition timescales determined the lifetime of atmospheric MPs. Table S2 shows the gravitational settling velocities (V_g) of MPs and compares them against the V_g of typical dust particles.[41] For the eight sizes/shapes of MPs represented in our model, the V_g of MP pellets (5.4 cm s^{-1} for P_{40} and 14 cm s^{-1} for P_{70}) were much larger than those of MP fragments (1.1 to 1.2 cm s^{-1}) and MP lines (1.4 to 2.1 cm s^{-1}). In comparison, the V_g of dust particles 1.4, 2.8, 4.8, 9.0, and 16 μm in diameter are 0.04, 0.15, 0.44, 1.6, and 5.0 cm s^{-1}, respectively. Despite their larger sizes, the atmospheric transportability of MP fragments and lines were comparable to those of coarse dust particles 9.0−16 μm in diameter. This was mainly due to the larger surface-area-to-volume ratios of MP fragments and lines, which increased their drag in the air. Also, the densities of atmospheric MPs (980−2200 kg m^{-3})[28,46] were approximately 37−83% of the density of dust particles (assumed to be 2650 kg m^{-3}).[30] The atmospheric transportability of MP pellets was limited due to their smaller drag in the air. We derived independent, order-of-magnitude estimates for the deposition rate of bulk atmospheric MPs using the ratio between the measured fluxes of deposited atmospheric MPs and the concentrations of suspended atmospheric MPs at Lianyungang and Tianjin, respectively (Table S1). These measurements were not made concurrently at each city and were analyzed using different methods. Nevertheless, these measurements indicated a bulk deposition velocity of atmospheric MPs of 0.6−5 cm s^{-1}, consistent with our aerodynamic calculations of V_g in terms of the order of magnitude.

If lifted to a 2 km altitude (approximate boundary layer top) and assuming a typical wind speed of 10 m s^{-1}, MP fragments and lines may be transported in the air for 1.1 to 2.1 days and over long distances of 970 to 1800 km before they gravitationally settle to the surface. In contrast, the MP pellets represented in our model may be transported for 0.17−0.43

https://doi.org/10.1021/acs.est.1c07825
Environ. Sci. Technol. 2022, 56, 6243−6252

days and over 150−370 km downwind, such that they mostly deposit near their point of emission (Table S2).

Atmospheric Emissions of MPs from Land and Marine Sources. Figure 1 and Table 1 show the tuned annual atmospheric emissions of MPs for our research domain for the year 2018. By mass, 12.5% of the total MPs (19.3, 8.0, and 1.9% of pellets, fragments, and lines, respectively) released to the continental Asian environment effectively entered the atmosphere (Table S5). Our tuned estimate for the annual atmospheric MPs emission from Asian land surfaces (within the domain of Figure 1) was 310 Gg for 2018, including 280, 8.1, and 17 Gg of MP pellets, fragments, and lines, respectively. The atmospheric emissions of MP pellets were the largest due to their emissions from tire dust (Figure S6 and Table S5).

Table 1. Annual Budgets of Atmospheric MPs over Asia and Adjacent Oceans (Domain Shown in Figure 1) for the Year 2018

MP shapes	pellets	fragments	lines	total MPs
Atmospheric emissions (Gg y^{-1})				
from land	*280*	*8.1*	*17*	*310*
from ocean	*56*	*1.6*	*3.4*	*60*
Suspended MP burden (Gg)	1.1	0.40	0.64	2.1
from land	*0.93*	*0.34*	*0.55*	*1.8*
from ocean	*0.16*	*0.058*	*0.093*	*0.31*
Deposited MP flux (Gg y^{-1})	340	9.3	20	370
over land	280	6.9	15	300
from land	*280*	*6.8*	*15*	*300*
from ocean	*0.097*	*0.10*	*0.15*	*0.35*
over ocean	57	2.3	4.5	64
from land	*2.0*	*0.88*	*1.3*	*4.2*
from ocean	*55*	*1.4*	*3.1*	*60*

Our tuned estimate for the annual atmospheric MP emission from the Northwestern Pacific and Indian oceans (within the domain of Figure 1) was 60 Gg for 2018, including 56, 1.6, and 3.4 Gg of MP pellets, fragments, and lines, respectively (Table 1). The marine emissions of MP pellets were largest due to our assumption that the MPs emitted from the ocean surface had the same morphology composition as the MPs emitted from land. Marine emissions of MPs into the atmosphere were highest in January (7.2 Gg) and lowest in April (3.0 Gg), modulated by seasonal wind speed variations (Figure S4 and Table S6).

Evaluation of Simulated Atmospheric MPs against Measurements in the Study Area. We evaluated our simulated atmospheric MP abundances against observations over Asia and its adjacent oceans (Figure 1). Figure 2a compares the observed and simulated deposited atmospheric MP fluxes at nine Asian coastal sites (Figure S1 and Table S1). The simulated deposited atmospheric MP fluxes at eight Chinese coastal cities ranged from 26 to 210 MPs m^{-2} day^{-1}, comparable to the observed fluxes of 36−245 MPs m^{-2} day^{-1}.[33−35] The simulated annual deposited atmospheric MP fluxes at Ho Chi Minh City, Vietnam, were 275−578 MPs m^{-2} day^{-1}, comparable to the observed fluxes at that location (383−537 MPs m^{-2} day^{-1}).[36] The correlation coefficient (r) between the observed and simulated deposited atmospheric MP fluxes was 0.92; the normalized mean bias (NMB) of the simulated fluxes was −8.7% (Figure S7a).

Figures 2b−e and S7b compare the observed and simulated suspended atmospheric MP concentrations at 9 Chinese coastal cities and 56 locations over the South China Sea and the East Indian Ocean. The observed suspended MP concentrations at the nine Chinese coastal cities ranged between 0.022 and 0.43 MPs m^{-3},[34] with the highest concentrations at Shanghai and Nantong (both in the Yangtze River Delta megacity cluster). Our simulated suspended MP concentrations at the nine Chinese coastal cities ranged between 0.024 and 0.39 MPs m^{-3} and were also highest at Shanghai and Nantong, in good agreement with the observations. The simulated suspended MP concentrations over the South China Sea and the Indian Ocean ranged between 0.0002 and 0.078 MPs m^{-3}, consistent with the observed ranges (0 and 0.077 MPs m^{-3}).[29,37,38] The simulated suspended MP numbers were generally consistent with measurements over Chinese coastal cities (r = 0.96, NMB = −1.0%; r = 0.35, NMB = −5.1% if excluding two extreme values, Figure S7b) and over the East Indian Ocean and the South China Sea (sites I1 to I21 in Figure 2e, r = 0.71, NMB = −33%). However, the simulated MP concentrations were less consistent with the near-shore measurements over the South China Sea (r = 0.27, NMB = 33%, Figure S7b). This lack of agreement may be partially due to the different sampling and analytical methods used by individual measurement teams. Our simulated suspended MP concentrations agreed better with measurements by Ding et al.[37] (sites S1 to S12 in Figure 2c, r = 0.71, NMB = −44%) but were higher than the measurements by Wang et al.[38] (sites S13 to S35 in Figure 2d, r = −0.24, NMB = 310%). Our simulation indicated that approximately 80% of suspended atmospheric MPs over the East Indian Ocean and the South China Sea were MP fibers, while the rest were MP fragments, consistent with the observations of Wang et al.[29]

Atmospheric Transports and Depositions of MPs over Asia and Adjacent Oceans. Our analyses above showed that the WRF-MP model generally reproduced the observed abundances and morphologies of atmospheric MPs over Asia and adjacent oceans. On that basis, we assessed the atmospheric transports and depositions of MPs over this region to quantify the regional source-to-sink relationship of MPs between lands and oceans.

Figure 3a−h shows our simulated annual mean surface suspended atmospheric MP concentrations from continental and marine sources. Over land, the simulated annual mean surface suspended atmospheric MP concentrations ranged from <0.001 MPs m^{-3} over the remote continental areas to >1 MPs m^{-3} over major cities. The simulated annual mean surface suspended MPs over Asia mostly consists of MP pellets (51% by mass), followed by MP lines (30%) and fragments (19%). Despite their dominant emissions (92% by mass), MP pellets only constituted half (51%) of the surface suspended atmospheric MPs over Asian lands and were rarely transported beyond the coastal waters. This discrepancy was because the MP pellets represented in our model were relatively large and quickly settled to the surface after emission. Continental-origin MP lines and fragments may be transported >1000 km into the marine atmosphere, where these continental-origin MPs became comparable in concentrations to the marine-origin MPs. Over the Northwestern Pacific and Indian oceans, the simulated annual mean surface suspended atmospheric MP concentrations ranged from 0 over the remote oceans to >0.05 MPs m^{-3} over polluted surface oceans (e.g., the Yellow Sea,

https://doi.org/10.1021/acs.est.1c07825
Environ. Sci. Technol. 2022, 56, 6243−6252

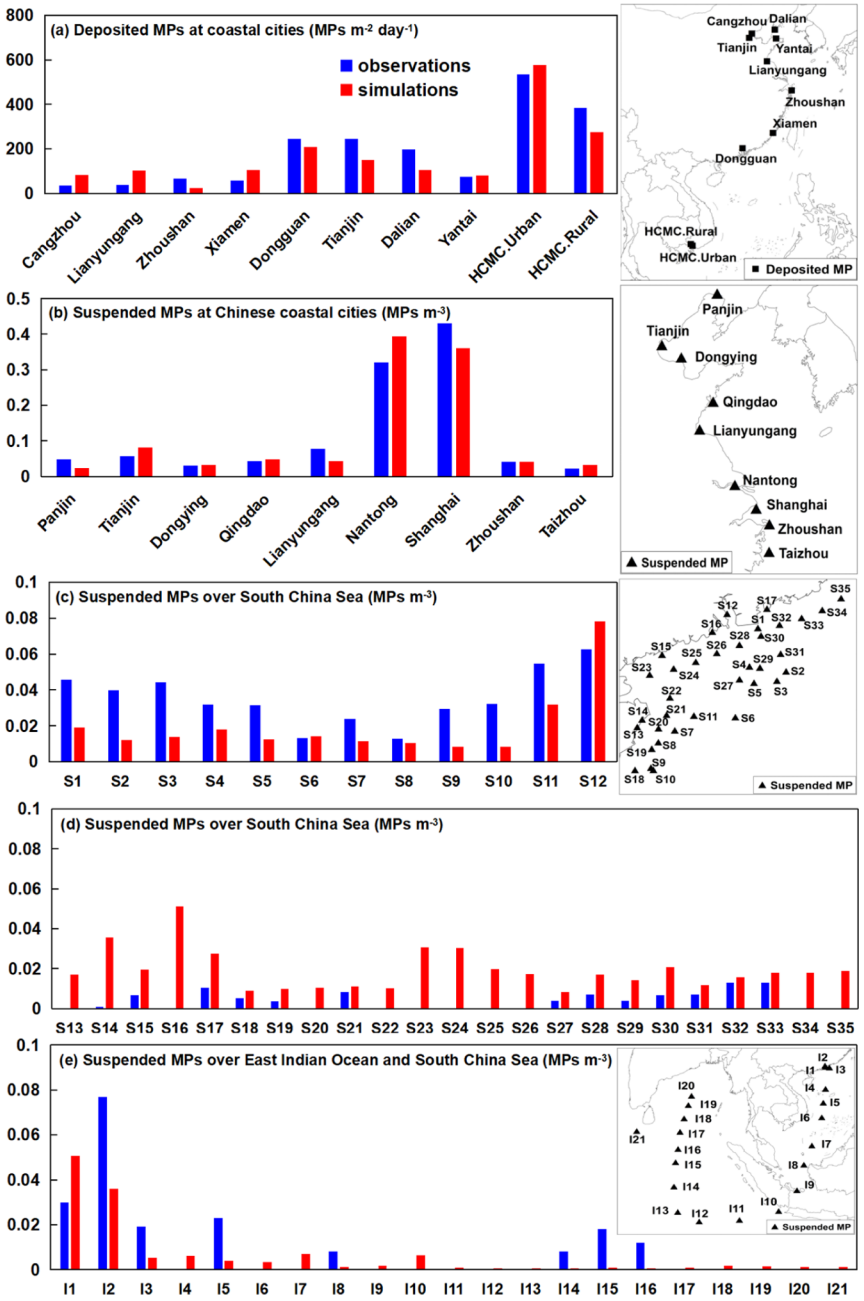

Figure 2. Comparison of the observed (blue bars) and simulated (red bars) (a) deposited atmospheric MP number fluxes at coastal locations[33−36] as well as the observed and simulated suspended atmospheric MP number concentrations (b) at Chinese coastal cities,[34] (c) and (d) over the South China Sea,[37,38] and (e) over the East Indian Ocean and the South China Sea.[29]

the East China Sea, the Sea of Japan, and the waters east of Japan). Marine-origin MPs, particularly MP lines, might be transported up to 500 km inland and comparable in concentrations to continental-origin MPs at very clean coastal land areas, such as Hokkaido, Japan, and Eastern Malaysia Peninsula.

Figure 3i−p shows the simulated annual mean surface deposited atmospheric MP fluxes from continental and marine sources. Over land, the simulated annual mean deposited atmospheric MP fluxes over densely populated areas exceeded 500 MPs m^{-2} day^{-1}, mostly reflecting the deposition of MP pellets near their sources. In comparison, the deposition of MPs from marine sources over land was insignificant. Over the oceans, the simulated annual mean deposited atmospheric MP fluxes ranged from 0 at remote locations to >200 MPs m^{-2} day^{-1} over polluted waters, mostly reflecting the local emission and deposition of MP pellets. However, MP fragments and lines from Asia were transported in the air and deposited as far as 170° E, >2000 km away from the Asian coast. Over the Asian coastal waters (<500 km from the coast), the deposited MP fluxes from continental sources may exceed 10 MPs m^{-2} day^{-1}, comparable to the marine contribution to the local deposited MP fluxes.

We found that the monsoonal climate modulated the emission and transport of MPs between Asia and its adjacent oceans (Figures S4 and S8). In January, MPs emitted from East and South Asia were effectively transported by the strong Asian winter monsoon to the Northwestern Pacific, the

https://doi.org/10.1021/acs.est.1c07825
Environ. Sci. Technol. 2022, 56, 6243−6252

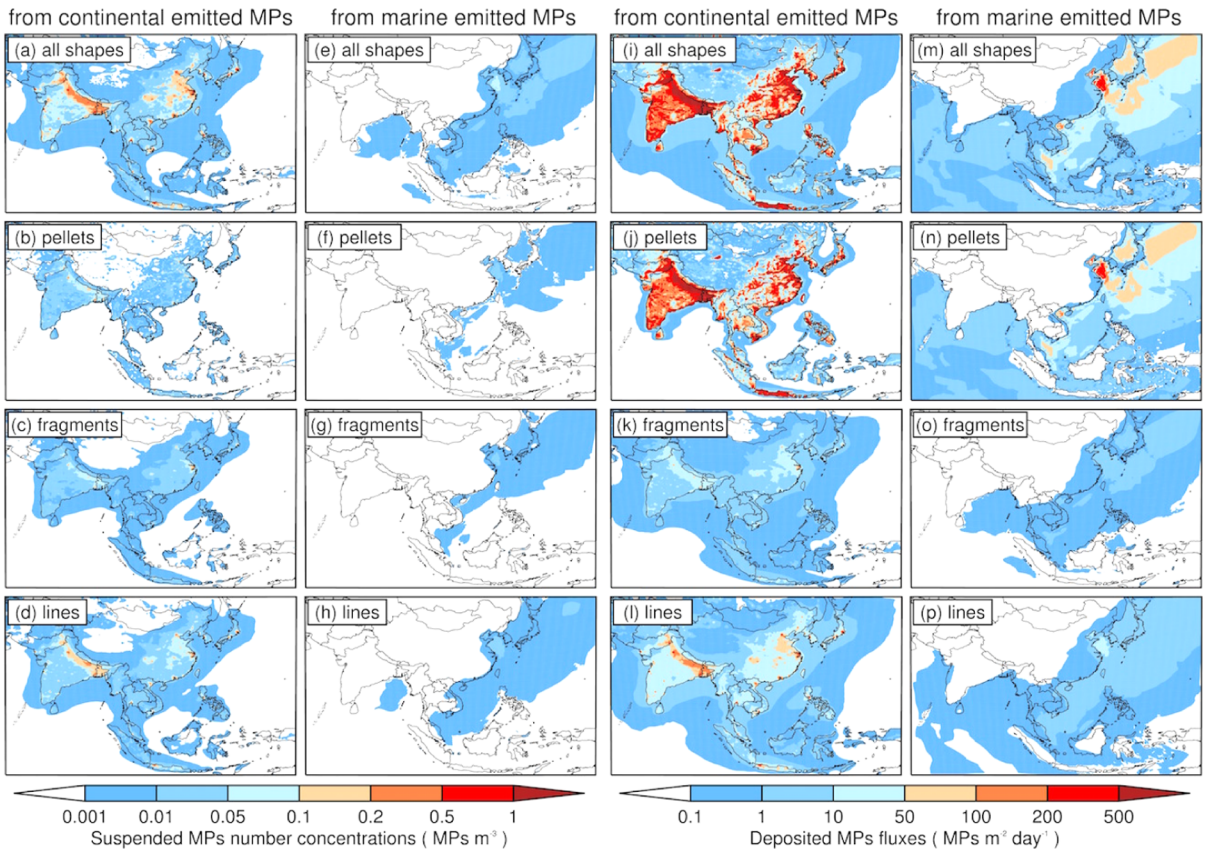

Figure 3. Simulated annual mean surface number concentrations of suspended atmospheric MPs (a−d) from continental and (e−h) marine sources; simulated annual mean surface deposited atmospheric MP fluxes (i−l) from continental and (m−p) marine sources. Both suspended atmospheric MP concentrations and deposited atmospheric MP fluxes are shown for MPs of all shapes and for MP pellets, fragments, and lines, respectively.

Equatorial Western Pacific, and the Equatorial Indian Ocean. In July, the prevailing southerly winds led to less transport of continental MPs from Asia to the oceans, while marine-origin MPs were more effectively transported toward Asia.

Table 1 summarizes the annual budgets of atmospheric MPs from Asia and adjacent oceans for the year 2018. The annual mean atmospheric burden of MPs in our simulated domain was 2.1 Gg, half of which was associated with MP pellets (1.1 Gg). The annual deposited atmospheric MP flux over Asian land surfaces was 300 Gg y^{-1}, almost entirely from continental sources. The annual deposited MP fluxes over the Northwestern Pacific and the Indian Oceans (within the domain of Figure 1) were 64 Gg y^{-1}, including 4.2 and 60 Gg y^{-1} from continental and marine sources, respectively. We estimated that 1.4% of the total atmospheric MP emissions by mass (0.70% for pellets, 11% for fragments, and 7.8% for lines) from land surfaces deposited to the ocean via atmospheric transport. A previous Lagrangian model study estimated that 15−16% of the mass of MP lines emitted into the global atmosphere was transported to the open ocean,[34] comparable with our mechanistic calculations for MP fragments and lines.

Comparison with Brahney et al.[30] We compared our simulated atmospheric deposition fluxes of MPs with those simulated by Brahney et al.[30] over our research domain (Figure S9). The annual atmospheric deposition fluxes of MPs simulated by us (370 Gg y^{-1}) and Brahney et al.[30] (440 Gg y^{-1}) were within 20% of each other. However, the attribution of the deposited MPs was very different: we attributed 310 Gg y^{-1} of deposited MP flux to continental sources, while Brahney et al.[30] attributed the bulk of their deposited MPs to marine sources (340 Gg y^{-1}). The reason for this discrepancy may be threefold: (1) Brahney et al.[30] constrained their atmospheric MP emissions with observations at 11 remote sites in the Western U.S. According to the calculated atmospheric residence times of MPs in both studies (0.43−2.1 days in this study and 0.04−6.5 days in Brahney et al.[30]), these Western U.S. measurements would mostly reflect emissions over the Western U.S. and Northeastern Pacific, where continental MP emissions might be smaller than those over East and South Asia. (2) The deposition samples at mountainous Western U.S. may be enhanced in MPs that were long-range-transported due to the stronger winds at high altitudes. (3) Finally, the size range of MPs represented in Brahney et al.[30] (0.3−70 μm) was much smaller than that represented in this study (~10 to 5000 μm). They may have underestimated the atmospheric transport of larger MPs, particularly those of MP lines and fragments. For these reasons, and because the observed suspended atmosphere MP concentrations showed a sharp decline from the Asian coast to the remote marine locations (Figure 2), continental-origin MPs more likely dominated the deposition fluxes of MPs over Asia and its adjacent oceans.

DISCUSSION

Given the exploratory nature of this study, it was difficult to quantify the uncertainty of our simulated atmospheric MP budget and the simulated land−sea MP flux. The uncertainty

https://doi.org/10.1021/acs.est.1c07825
Environ. Sci. Technol. 2022, 56, 6243−6252

of the total environmental MP release was a factor of 2.[13,50] However, the atmospheric MP emissions in our model were an effective mixture of primary, secondary, and re-suspended sources. We did not explicitly represent breakdown/aging processes of primary MPs in terrestrial and aquatic environments. These uncertainties were effectively represented by the uncertainty associated with α_i, which we tuned to a mean value of 12.5% (Table S5).

We roughly estimated the uncertainty of our simulated atmospheric MP budget to be between factors of 3 and 7, based on the following "top-down" and "bottom-up" considerations. First, our simulated suspended MP concentrations and deposited MP fluxes were within a factor of 3 of the available observations (Figure S7). Second, Wang et al.[50] estimated that one-sixth of the environmental MP emission over land entered the aquatic environment. Assuming that the rest of the MPs all entered the atmosphere, we estimated an upper-limit for α_i of 83%, resulting in a factor of 7 uncertainty in the value of α_i.

Our estimated net flux of MPs from the Asian continent (domain in Figure 1) to the oceans via atmospheric transport was 3.9 Gg y^{-1}. A previous estimate for the annual riverine source of MPs from East and South Asia to the oceans was 20 Gg y^{-1}.[58] However, 90% of that estimated riverine source was in the form of transported macroplastics (plastic debris > 5 mm), which fragmented into MPs in the ocean. The riverine transport of actual MPs from East and South Asia to the oceans was estimated to be 2 Gg y^{-1}.[58] Therefore, our study indicated that atmospheric transport was the major pathway by which MPs were transported from land to oceans over our domain of interest. Because atmospheric transports are strongly linked to weather and large-scale atmospheric circulations, the atmospheric transport of MPs is likely a more dynamic and variable migration pathway of MPs from their source to other parts of the world. More measurements and experimental studies are needed to constrain the sizes, morphologies, and fluxes of MPs in the atmosphere, the aging and breakdown of MPs in terrestrial and aquatic environments, and the retention and re-suspension of MPs from land and ocean surfaces, to construct a more complete mechanistic understanding of the global MP cycle and its impacts on the ecosystems.

■ ASSOCIATED CONTENT

Supporting Information

The Supporting Information is available free of charge at https://pubs.acs.org/doi/10.1021/acs.est.1c07825.

Additional materials about the observations used in this study, the WRF-MP model, MP emissions, model results, and comparison with previous studies (PDF)

■ AUTHOR INFORMATION

Corresponding Author

Tzung-May Fu − *State Environmental Protection Key Laboratory of Integrated Surface Water-Groundwater Pollution Control, School of Environmental Science and Engineering, Southern University of Science and Technology, Shenzhen, Guangdong 518055, China; Guangdong Provincial Observation and Research Station for Coastal Atmosphere and Climate of the Greater Bay Area, Shenzhen, Guangdong 518055, China;* orcid.org/0000-0002-8556-7326; Email: fuzm@sustech.edu.cn

Authors

Xin Long − *State Environmental Protection Key Laboratory of Integrated Surface Water-Groundwater Pollution Control, School of Environmental Science and Engineering, Southern University of Science and Technology, Shenzhen, Guangdong 518055, China; Guangdong Provincial Observation and Research Station for Coastal Atmosphere and Climate of the Greater Bay Area, Shenzhen, Guangdong 518055, China;* orcid.org/0000-0002-6272-4712

Xin Yang − *State Environmental Protection Key Laboratory of Integrated Surface Water-Groundwater Pollution Control, School of Environmental Science and Engineering, Southern University of Science and Technology, Shenzhen, Guangdong 518055, China; Guangdong Provincial Observation and Research Station for Coastal Atmosphere and Climate of the Greater Bay Area, Shenzhen, Guangdong 518055, China;* orcid.org/0000-0002-9173-1188

Yuanyuan Tang − *State Environmental Protection Key Laboratory of Integrated Surface Water-Groundwater Pollution Control, School of Environmental Science and Engineering, Southern University of Science and Technology, Shenzhen, Guangdong 518055, China*

Yan Zheng − *State Environmental Protection Key Laboratory of Integrated Surface Water-Groundwater Pollution Control, School of Environmental Science and Engineering, Southern University of Science and Technology, Shenzhen, Guangdong 518055, China;* orcid.org/0000-0001-5256-9395

Lei Zhu − *State Environmental Protection Key Laboratory of Integrated Surface Water-Groundwater Pollution Control, School of Environmental Science and Engineering, Southern University of Science and Technology, Shenzhen, Guangdong 518055, China; Guangdong Provincial Observation and Research Station for Coastal Atmosphere and Climate of the Greater Bay Area, Shenzhen, Guangdong 518055, China*

Huizhong Shen − *State Environmental Protection Key Laboratory of Integrated Surface Water-Groundwater Pollution Control, School of Environmental Science and Engineering, Southern University of Science and Technology, Shenzhen, Guangdong 518055, China; Guangdong Provincial Observation and Research Station for Coastal Atmosphere and Climate of the Greater Bay Area, Shenzhen, Guangdong 518055, China*

Jianhuai Ye − *State Environmental Protection Key Laboratory of Integrated Surface Water-Groundwater Pollution Control, School of Environmental Science and Engineering, Southern University of Science and Technology, Shenzhen, Guangdong 518055, China; Guangdong Provincial Observation and Research Station for Coastal Atmosphere and Climate of the Greater Bay Area, Shenzhen, Guangdong 518055, China*

Chen Wang − *State Environmental Protection Key Laboratory of Integrated Surface Water-Groundwater Pollution Control, School of Environmental Science and Engineering, Southern University of Science and Technology, Shenzhen, Guangdong 518055, China; Guangdong Provincial Observation and Research Station for Coastal Atmosphere and Climate of the Greater Bay Area, Shenzhen, Guangdong 518055, China;* orcid.org/0000-0001-9565-8777

Teng Wang − *College of Oceanography, Hohai University, Nanjing, Jiangsu 210098, China*

Baojie Li − *School of Environmental Science and Engineering, Nanjing University of Information Science and Technology, Nanjing, Jiangsu 210044, China;* orcid.org/0000-0002-3747-6534

https://doi.org/10.1021/acs.est.1c07825
Environ. Sci. Technol. 2022, 56, 6243−6252

Complete contact information is available at:
https://pubs.acs.org/10.1021/acs.est.1c07825

Funding

X.L. and T.-M.F. conducted the modeling and analyses. T.W. and B.L. provided the MP emissions over Mainland China. X.Y., Y.T., Y.Z., L.Z., H.S., J.Y., and C.W. assisted in the interpretation of the results. All authors discussed the findings and contributed to the paper.

Notes

The authors declare no competing financial interest.

■ ACKNOWLEDGMENTS

We thank Daoji Li and Kai Liu of East China Normal University for providing the MP measurements over the Pacific. This work was supported by the National Natural Science Foundation of China (41907191, 41975158), the Guangdong Basic and Applied Basic Research Fund (2020B1515130003), and the Shenzhen Science and Technology Innovation Committee (KCXFZ202002011008038, JCYJ20190809144601730). Computational resources were provided by the Center for Computational Science and Engineering at Southern University of Science and Technology.

■ REFERENCES

(1) Joint Group of Experts on the Scientific Aspects of Marine Environmental Protection. Guildelines for the Monitoring and Assessment of Plastic Litter in the Ocean. Kershaw, P.; Turra, A.; Galgani, F., Eds.; *Rep. Stud. - GESAMP* 2019, Vol. *99*, 123p.

(2) Auta, H. S.; Emenike, C. U.; Fauziah, S. H. Distribution and importance of microplastics in the marine environment: a review of the sources, fate, effects, and potential solutions. *Environ. Int.* **2017**, *102*, 165−176.

(3) Jâms, I. B.; Windsor, F. M.; Poudevigne-Durance, T.; Ormerod, S. J.; Durance, I. Estimating the size distribution of plastics ingested by animals. *Nat. Commun.* **2020**, *11*, 1594.

(4) Li, J.; Liu, H.; Paul Chen, J. Microplastics in freshwater systems: a review on occurrence, environmental effects, and methods for microplastics detection. *Water Res.* **2018**, *137*, 362−374.

(5) Ragusa, A.; Svelato, A.; Santacroce, C.; Catalano, P.; Notarstefano, V.; Carnevali, O.; Papa, F.; Rongioletti, M. C. A.; Baiocco, F.; Draghi, S.; D'Amore, E.; Rinaldo, D.; Matta, M.; Giorgini, E. Plasticenta: first evidence of microplastics in human placenta. *Environ. Int.* **2021**, *146*, 106274.

(6) Koelmans, A. A.; Redondo-Hasselerharm, P. E.; Nor, N. H. M.; de Ruijter, V. N.; Mintenig, S. M.; Kooi, M. Risk assessment of microplastic particles. *Nat. Rev. Mater.* **2022**, *7*, 138−152.

(7) Beiras, R.; Bellas, J.; Cachot, J.; Cormier, B.; Cousin, X.; Engwall, M.; Gambardella, C.; Garaventa, F.; Keiter, S.; Le Bihanic, F.; López-Ibáñez, S.; Piazza, V.; Rial, D.; Tato, T.; Vidal-Liñán, L. Ingestion and contact with polyethylene microplastics does not cause acute toxicity on marine zooplankton. *J. Hazard. Mater.* **2018**, *360*, 452−460.

(8) Beiras, R.; Tato, T. Microplastics do not increase toxicity of a hydrophobic organic chemical to marine plankton. *Mar. Pollut. Bull.* **2019**, *138*, 58−62.

(9) Cole, M.; Lindeque, P.; Fileman, E.; Halsband, C.; Galloway, T. S. The impact of polystyrene microplastics on feeding, function and fecundity in the marine copepod Calanus helgolandicus. *Environ. Sci. Technol.* **2015**, *49*, 1130−1137.

(10) Martínez-Gómez, C.; León, V. M.; Calles, S.; Gomáriz-Olcina, M.; Vethaak, A. D. The adverse effects of virgin microplastics on the fertilization and larval development of sea urchins. *Mar. Environ. Res.* **2017**, *130*, 69−76.

(11) Ribeiro, F.; Garcia, A. R.; Pereira, B. P.; Fonseca, M.; Mestre, N. C.; Fonseca, T. G.; Ilharco, L. M.; Bebianno, M. J. Microplastics effects in Scrobicularia plana. *Mar. Pollut. Bull.* **2017**, *122*, 379−391.

(12) Borrelle, S. B.; Ringma, J.; Law, K. L.; Monnahan, C. C.; Lebreton, L.; McGivern, A.; Murphy, E.; Jambeck, J.; Leonard, G. H.; Hilleary, M. A.; Eriksen, M.; Possingham, H. P.; De Frond, H.; Gerber, L. R.; Polidoro, B.; Tahir, A.; Bernard, M.; Mallos, N.; Barnes, M.; Rochman, C. M. Predicted growth in plastic waste exceeds efforts to mitigate plastic pollution. *Science* **2020**, *369*, 1515−1518.

(13) Boucher, J.; Friot, D. *Primary Microplastics in the Oceans: A Global Evaluation of Sources*; IUCN: Gland, Switzerland, 2017; p 43.

(14) Xu, C.; Zhang, B.; Gu, C.; Shen, C.; Yin, S.; Aamir, M.; Li, F. Are we underestimating the sources of microplastic pollution in terrestrial environment? *J. Hazard. Mater.* **2020**, *400*, 123228.

(15) Brahney, J.; Hallerud, M.; Heim, E.; Hahnenberger, M.; Sukumaran, S. Plastic rain in protected areas of the United States. *Science* **2020**, *368*, 1257−1260.

(16) Siegfried, M.; Koelmans, A. A.; Besseling, E.; Kroeze, C. Export of microplastics from land to sea. A modelling approach. *Water Res.* **2017**, *127*, 249−257.

(17) Barboza, L. G. A.; Gimenez, B. C. G. Microplastics in the marine environment: current trends and future perspectives. *Mar. Pollut. Bull.* **2015**, *97*, 5−12.

(18) Cózar, A.; Echevarría, F.; González-Gordillo, J. I.; Irigoien, X.; Úbeda, B.; Hernández-León, S.; Palma, Á. T.; Navarro, S.; García-de-Lomas, J.; Ruiz, A. Plastic debris in the open ocean. *Proc. Natl. Acad. Sci. U.S.A.* **2014**, *111*, 10239−10244.

(19) Hale, R. C.; Seeley, M. E.; Guardia, M. J. L.; Mai, L.; Zeng, E. Y. A global perspective on microplastics. *J. Geophys. Res. C Oceans* **2020**, *125*, No. e2018JC014719.

(20) Zarfl, C.; Fleet, D.; Fries, E.; Galgani, F.; Gerdts, G.; Hanke, G.; Matthies, M. Microplastics in oceans. *Mar. Pollut. Bull.* **2011**, *62*, 1589−1591.

(21) Zhang, Y.; Kang, S.; Allen, S.; Allen, D.; Gao, T.; Sillanpää, M. Atmospheric microplastics: a review on current status and perspectives. *Earth-Sci. Rev.* **2020**, *203*, 103118.

(22) Allen, S.; Allen, D.; Phoenix, V. R.; Le Roux, G.; Durántez Jiménez, P.; Simonneau, A.; Binet, S.; Galop, D. Atmospheric transport and deposition of microplastics in a remote mountain catchment. *Nat. Geosci.* **2019**, *12*, 339−344.

(23) Napper, I. E.; Davies, B. F. R.; Clifford, H.; Elvin, S.; Koldewey, H. J.; Mayewski, P. A.; Miner, K. R.; Potocki, M.; Elmore, A. C.; Gajurel, A. P.; Thompson, R. C. Reaching new heights in plastic pollution—preliminary findings of microplastics on Mount Everest. *One Earth* **2020**, *3*, 621−630.

(24) Aves, A. R.; Revell, L. E.; Gaw, S.; Ruffell, H.; Schuddeboom, A.; Wotherspoon, N. E.; LaRue, M.; McDonald, A. J. First evidence of microplastics in Antarctic snow. *Cryosphere Discuss.* **2022**, *2022*, 1−31.

(25) Bergmann, M.; Mützel, S.; Primpke, S.; Tekman, M. B.; Trachsel, J.; Gerdts, G. White and wonderful? Microplastics prevail in snow from the Alps to the Arctic. *Sci. Adv.* **2019**, *5*, No. eaax1157.

(26) Adams, J. K.; Dean, B. Y.; Athey, S. N.; Jantunen, L. M.; Bernstein, S.; Stern, G.; Diamond, M. L.; Finkelstein, S. A. Anthropogenic particles (including microfibers and microplastics) in marine sediments of the Canadian Arctic. *Sci. Total Environ.* **2021**, *784*, 147155.

(27) Huntington, A.; Corcoran, P. L.; Jantunen, L.; Thaysen, C.; Bernstein, S.; Stern, G. A.; Rochman, C. M. A first assessment of microplastics and other anthropogenic particles in Hudson Bay and the surrounding eastern Canadian Arctic waters of Nunavut. *Facets* **2020**, *5*, 615−616.

(28) Liu, K.; Wu, T.; Wang, X.; Song, Z.; Zong, C.; Wei, N.; Li, D. Consistent transport of terrestrial microplastics to the ocean through atmosphere. *Environ. Sci. Technol.* **2019**, *53*, 10612−10619.

(29) Wang, X.; Li, C.; Liu, K.; Zhu, L.; Song, Z.; Li, D. Atmospheric microplastic over the South China Sea and East Indian Ocean: abundance, distribution and source. *J. Hazard. Mater.* **2020**, *389*, 121846.

(30) Brahney, J.; Mahowald, N.; Prank, M.; Cornwell, G.; Klimont, Z.; Matsui, H.; Prather, K. A. Constraining the atmospheric limb of the plastic cycle. *Proc. Natl. Acad. Sci. U.S.A.* **2021**, *118*, No. e2020719118.
(31) Evangeliou, N.; Grythe, H.; Klimont, Z.; Heyes, C.; Eckhardt, S.; Lopez-Aparicio, S.; Stohl, A. Atmospheric transport, a major pathway of microplastics to remote regions. *Nat. Commun.* **2020**, *11*, 3381.
(32) Rochman, C. M.; Brookson, C.; Bikker, J.; Djuric, N.; Earn, A.; Bucci, K.; Athey, S.; Huntington, A.; McIlwraith, H.; Munno, K.; De Frond, H.; Kolomijeca, A.; Erdle, L.; Grbic, J.; Bayoumi, M.; Borrelle, S. B.; Wu, T.; Santoro, S.; Werbowski, L. M.; Zhu, X.; Giles, R. K.; Hamilton, B. M.; Thaysen, C.; Kaura, A.; Klasios, N.; Ead, L.; Kim, J.; Sherlock, C.; Ho, A.; Hung, C. Rethinking microplastics as a diverse contaminant suite. *Environ. Toxicol. Chem.* **2019**, *38*, 703−711.
(33) Cai, L.; Wang, J.; Peng, J.; Tan, Z.; Zhan, Z.; Tan, X.; Chen, Q. Characteristic of microplastics in the atmospheric fallout from Dongguan city, China: preliminary research and first evidence. *Environ. Sci. Pollut. Res.* **2017**, *24*, 24928−24935.
(34) Liu, K.; Wang, X.; Song, Z.; Wei, N.; Ye, H.; Cong, X.; Zhao, L.; Li, Y.; Qu, L.; Zhu, L.; Zhang, F.; Zong, C.; Jiang, C.; Li, D. Global inventory of atmospheric fibrous microplastics input into the ocean: an implication from the indoor origin. *J. Hazard. Mater.* **2020**, *400*, 123223.
(35) Tian, Y.; Tu, C.; Zhou, Q.; Zhang, C.; Li, L.; Tian, C.; Zong, Z.; Luo, Y. The temporal and spatial distribution and surface morphology of atmospheric microplastics around the Bohai Sea. *Acta Sci. Circumstantiae* **2020**, *40*, 1401−1409.
(36) Truong, T.-N.-S.; Strady, E.; Kieu-Le, T.-C.; Tran, Q.-V.; Le, T.-M. -T.; Thuong, Q.-T. Microplastic in atmospheric fallouts of a developing Southeast Asian megacity under tropical climate. *Chemosphere* **2021**, *272*, 129874.
(37) Ding, Y.; Zou, X.; Wang, C.; Feng, Z.; Wang, Y.; Fan, Q.; Chen, H. The abundance and characteristics of atmospheric microplastic deposition in the northwestern South China Sea in the fall. *Atmos. Environ.* **2021**, *253*, 118389.
(38) Wang, X.; Liu, K.; Zhu, L.; Li, C.; Song, Z.; Li, D. Efficient transport of atmospheric microplastics onto the continent via the East Asian summer monsoon. *J. Hazard. Mater.* **2021**, *414*, 125477.
(39) Ginoux, P.; Chin, M.; Tegen, I.; Prospero, J. M.; Lin, S.-J. Sources and global distributions of dust aerosols simulated with the GOCART model. *J. Geophys. Res. Atmos.* **2001**, *106*, 20255−20273.
(40) Grell, G. A.; Peckham, S. E.; Schmitz, R.; McKeen, S. A.; Frost, G.; Skamarock, W. C.; Eder, B. Fully coupled "online" chemistry within the WRF model. *Atmos. Environ.* **2005**, *39*, 6957−6975.
(41) Bian, H.; Tie, X.; Cao, J.; Ying, Z.; Han, S.; Xue, Y. Analysis of a severe dust storm event over china: application of the WRF-Dust model. *Aerosol Air Qual. Res.* **2011**, *11*, 419−428.
(42) Legrand, S. L.; Polashenski, C.; Letcher, T. W.; Creighton, G. A.; Peckham, S. E.; Cetola, J. D. The AFWA dust emission scheme for the GOCART aerosol model in WRF-Chem v3.8.1. *Geosci. Model Dev.* **2019**, *12*, 131−166.
(43) Long, X.; Tie, X.; Li, G.; Cao, J.; Feng, T.; Zhao, S.; Xing, L.; An, Z. Effect of ecological restoration programs on dust concentrations in the North China Plain: a case study. *Atmos. Chem. Phys.* **2018**, *18*, 6353−6366.
(44) Bagheri, G.; Bonadonna, C. On the drag of freely falling non-spherical particles. *Powder Technol.* **2016**, *301*, 526−544.
(45) Bagheri, G.; Bonadonna, C. Erratum to "On the drag of freely falling non-spherical particles". *Powder Technol.* **2019**, *349*, 108.
(46) Liu, K.; Wang, X.; Fang, T.; Xu, P.; Zhu, L.; Li, D. Source and potential risk assessment of suspended atmospheric microplastics in Shanghai. *Sci. Total Environ.* **2019**, *675*, 462−471.
(47) Latto, B.; Saunders, M. W. Absolute viscosity of air down to cryogenic temperatures and up to high pressures. *Arch. Mech. Eng.* **1973**, *15*, 266−270.
(48) Bain, A.; Preston, T. C. Hygroscopicity of Microplastic and Mixed Microplastic Aqueous Ammonium Sulfate Systems. *Environ. Sci. Technol.* **2021**, *55*, 11775−11783.
(49) Kalnay, E.; Kanamitsu, M.; Kistler, R.; Collins, W.; Deaven, D.; Gandin, L.; Iredell, M.; Saha, S.; White, G.; Woollen, J.; Zhu, Y.; Leetmaa, A.; Reynolds, R.; Chelliah, M.; Ebisuzaki, W.; Higgins, W.; Janowiak, J.; Mo, K. C.; Ropelewski, C.; Wang, J.; Jenne, R.; Joseph, D. The NCEP/NCAR 40-Year Reanalysis Project. *Bull. Am. Meteorol. Soc.* **1996**, *77*, 437−471.
(50) Wang, T.; Li, B.; Zou, X.; Wang, Y.; Li, Y.; Xu, Y.; Mao, L.; Zhang, C.; Yu, W. Emission of primary microplastics in mainland China: invisible but not negligible. *Water Res.* **2019**, *162*, 214−224.
(51) Oak Ridge National Laboratory (ORNL). LandScan Global Population 2015 Database. https://landscan.ornl.gov/ (accessed on Feb 18, 2021).
(52) Garside, M. Production of plastics worldwide from 1950 to 2018. https://www.statista.com/statistics/282732/global-production-of-plastics-since-1950/ (accessed on Feb 18, 2021).
(53) Cheung, P. K.; Fok, L. Characterisation of plastic microbeads in facial scrubs and their estimated emissions in Mainland China. *Water Res.* **2017**, *122*, 53−61.
(54) Allen, S.; Allen, D.; Moss, K.; Le Roux, G.; Phoenix, V. R.; Sonke, J. E. Examination of the ocean as a source for atmospheric microplastics. *PLoS One* **2020**, *15*, No. e0232746.
(55) Monahan, E. C.; Spiel, D. E.; Davidson, K. L. *A Model of Marine Aerosol Generation via Whitecaps and Wave Disruption*; Springer Netherlands, 1986.
(56) van Sebille, E.; Wilcox, C.; Lebreton, L.; Maximenko, N.; Hardesty, B. D.; van Franeker, J. A.; Eriksen, M.; Siegel, D.; Galgani, F.; Law, K. L. A global inventory of small floating plastic debris. *Environ. Res. Lett.* **2015**, *10*, 124006.
(57) Fei, K.-C.; Wu, L.; Zeng, Q.-C. Aerosol optical depth and burden from large sea salt particles. *J. Geophys. Res. Atmos.* **2019**, *124*, 1680−1696.
(58) van Wijnen, J.; Ragas, A. M. J.; Kroeze, C. Modelling global river export of microplastics to the marine environment: sources and future trends. *Sci. Total Environ.* **2019**, *673*, 392−401.

https://doi.org/10.1021/acs.est.1c07825
Environ. Sci. Technol. 2022, 56, 6243−6252